Effects of Unstable Dark Matter on Large-Scale Structure and Constraints from Future Surveys

Mei-Yu Wang and Andrew R. Zentner

Department of Physics and Astronomy & Pittsburgh Particle physics,
Astrophysics, and Cosmology Center (PITT PACC),
The University of Pittsburgh, Pittsburgh, PA 15260 *

(Dated: January 13, 2012)

In this paper we explore the effect of decaying dark matter (DDM) on large-scale structure and possible constraints from galaxy imaging surveys. DDM models have been studied, in part, as a way to address apparent discrepancies between the predictions of standard cold dark matter models and observations of galactic structure. Our study is aimed at developing independent constraints on these models. In such models, DDM decays into a less massive, stable dark matter (SDM) particle and a significantly lighter particle. The small mass splitting between the parent DDM and the daughter SDM provides the SDM with a recoil or "kick" velocity v_k, inducing a free-streaming suppression of matter fluctuations. This suppression may be probed via weak lensing power spectra measured by a number of forthcoming imaging surveys that aim primarily to constrain dark energy. Using scales on which linear perturbation theory alone is valid (multipoles $\ell < 300$), surveys like Euclid or LSST can be sensitive to $v_k \gtrsim 90$ km/s for lifetimes $\tau \sim 1 - 5$ Gyr. To estimate more aggressive constraints, we model nonlinear corrections to lensing power using a simple halo evolution model that is in good agreement with numerical simulations. In our most ambitious forecasts, using multipoles $\ell < 3000$, we find that imaging surveys can be sensitive to $v_k \sim 10$ km/s for lifetimes $\tau \lesssim 10$ Gyr. Lensing will provide a particularly interesting complement to existing constraints in that they will probe the long lifetime regime ($\tau \gg H_0^{-1}$) far better than contemporary techniques. A caveat to these ambitious forecasts is that the evolution of perturbations on nonlinear scales will need to be well calibrated by numerical simulations before they can be realized. This work motivates the pursuit of such a numerical simulation campaign to constrain dark matter with cosmological weak lensing.

PACS numbers: 95.35.+d,98.80.-k,98.62.Gq,

I. INTRODUCTION

Many and various astronomical observations indicate that $\sim 5/6$ of the mass density of the Universe is non-baryonic *dark matter* (reviews include Refs. [1–3]). The simplest model of so-called *cold* dark matter (CDM) can be successfully applied to interpret an enormous amount of observational data, particularly those characterizing the large-scale ($\gtrsim$ a few Mpc) structure of the Universe and the gross properties of galaxies. In particular, the CDM model is consistent with the cosmic microwave background (CMB) anisotropy spectrum measured by the Wilkinson Microwave Anisotropy Probe (WMAP) and observations of the large-scale ($k \lesssim 0.1$ h/Mpc) galaxy clustering spectrum measured by the Sloan Digital Sky Survey (SDSS) [4]. On smaller scales, the situation is murkier. Several observations indicate possible discrepancies between CDM theory and observations on smaller scales. Among these are the well-known *missing satellites problem* [5, 6] and the steep rotation curves of low-surface brightness galaxies [7–9]. Exploring small-scale structure is challenging both observationally and theoretically. On the theoretical side, it is necessary to model highly non-linear phenomena to predict the properties of galaxies

and the dark matter halos in which they reside. Nevertheless, these potential shortcomings of CDM may point toward novel properties of dark matter and many alternatives to CDM have been considered, including *warm* dark matter (WDM) [10–14] and self-interacting dark matter (SIDM) [15–17].

As one alternative to CDM, unstable dark matter has been considered in a number of recent studies [15, 17–25]. In such models, a dark matter particle of mass M decays into a less massive daughter particle of mass $m = (1 - f) M$ and a significantly lighter, relativistic particle, with a lifetime on the order of the age of the Universe. In decaying dark matter models, cosmological structure growth is altered in a time- and scale-dependent manner [20, 26]. We explored models with $f \simeq 1$ in a previous paper [26]. If $f \ll 1$, the stable dark matter (SDM) daughter particle will receive a non-relativistic *kick* velocity, $v_k \simeq f c$. This kick can be sufficient to alter small-scale structure growth, modifying the predicted structures and abundances of the dark matter halos that host galaxies. Previous studies have explored just this possibility and placed limits on these scenarios by demanding that the alterations to structure growth not be so severe as to destroy the successes that CDM theory enjoys on large scales. An upper bound on the lifetime of the decaying dark matter (DDM) particle of $\tau \gtrsim 30 - 40$ Gyr for $v_k \gtrsim 100$ km/s can be derived from the observed galaxy-cluster mass function and

*Electronic address: mew56@pitt.edu,zentner@pitt.edu

galaxy mass-concentration relation [15, 17]. Lifetimes $\tau \lesssim 30$ Gyr with 20 km/s $\lesssim v_k \lesssim 200$ km/s may be in tension with the observed properties of the Milky Way satellite galaxy population, but uncertainties associated with the details of nonlinear structure growth in these models as well as the star formation histories of Local Group galaxies are significant [22]. Significantly tighter constraints can be obtained if the daughter particles are standard model particles [23].

With a number of forthcoming large-scale galaxy surveys being undertaken this decade, such as the Dark Energy Survey (DES)[1], the Panoramic Survey Telescope and Rapid Response System (Pan STARRS) [2], the Large Synoptic Survey Telescope (LSST)[3] [27], Euclid[4] [28], and WFIRST[5], it will be possible to investigate possible subtle imprints of decaying dark matter on the relatively large-scale structure of the Universe. In DDM models, the kick velocity at decay imparts upon the stable daughter particles the ability to smooth gravitational potential perturbations on scales smaller than the classic free-streaming scale. This behavior is similar to the cosmological influence of massive neutrinos or WDM, and numerous studies have shown that these features may be detectable in large-scale structure through galaxy clustering [29], Lyman-α forest [30–32], and cosmological weak lensing [33–35].

In this paper, we explore the effect of DDM model on large-scale structure and study the possible independent constraints on these models from forthcoming weak lensing surveys. There are distinct advantages to this approach. First, DDM models are explored largely in order to mitigate the possible small-scale problems of CDM, so it is necessary to explore independent predictions and probes in order to test such models. Second, the effects of DDM on large-scale structure, and on weak lensing power spectra in particular, are simpler to model in that they do not require detailed knowledge of galaxy formation in the highly nonlinear regime including star formation histories, star formation and active galaxy feedback, scale-dependent galaxy clustering bias and numerous other complicated phenomena that are known to be important on small scales. Third, many surveys already have the goal of measuring cosmological weak lensing as a probe of dark energy [36], so this test can be performed largely with the observational infrastructure used to study dark energy at no additional cost. Lyman-α forest spectra provide an additional, promising method to constrain DDM, but also introduce complications associated with modeling the clustering of neutral hydrogen along lines of sight to high redshift. We will present Lyman-α constraints on DDM, and forecasts for future measurements of the Lyman-α forest, in a forthcoming follow-up paper.

In the following sections, we will show that the imprint of DDM on lensing power spectra is sufficiently distinct from other cosmological parameters, such as neutrino mass, that one can disentangle degeneracies among them. Indeed, forthcoming data will be able to disentangle the two parameters of DDM models, lifetime and kick velocity (or equivalently f). Finally, large-scale lensing surveys will provide, at minimum, competitive and independent constraints on DDM models exploiting only scales on which linear cosmological perturbation theory is appropriate. These probes will have the particular advantage of probing significantly larger DDM lifetimes than small-scale structure studies and will not require detailed modeling of galaxy formation. Moreover, a relatively modest numerical simulation program may enable one to use mildly nonlinear scales $k \lesssim 1$ h/Mpc to obtain constraints on DDM that exceed current constraints and are robust to uncertainties associated with star formation and feedback in small galaxies.

The outline of this paper is as follows. In § II, we describe cosmological weak lensing observables. In § III, we discuss the perturbation evolution of both the parent and daughter particles in DDM models. In § IV, we study the effect of DDM on dark matter halo density profiles and explore possible influences of DDM on nonlinear structure. In § V, we describe the methods we use to compute constraints on DDM model parameters. We present our results in § VI, beginning with the general effects of DDM on large-scale structure, including a detailed discussion of the free-streaming of the daughter SDM particles. We also give our forecasts for constraints on DDM from large-scale weak lensing surveys and compare possible future bounds with existing limits. In § VII we summarize our work.

II. WEAK GRAVITATIONAL LENSING OBSERVABLES

Weak lensing as a cosmological probe has been discussed at length in numerous papers (a recent review is Ref. [37]). We give a brief description of our methods below, which are based on the conventions and notation in Ref. [38]. The most robust forecasts derive from considerations of possible weak lensing measurements restricted to scales where linear perturbative evolution of the metric potentials remains useful. However, we attempt to estimate possible improvements to the constraining power of weak lensing observables, provided that mildly nonlinear evolution can be modeled robustly.

We consider the set of observables that may be available from large-scale galaxy imaging surveys to be the auto- and cross-spectra of lensing convergence from sets of galaxies in N_{TOM} redshift bins. The $N_{TOM}(N_{TOM} + 1)/2$ distinct convergence spectra are

$$P_\kappa^{ij}(\ell) = \int dz \frac{W_i(z)W_j(z)}{H(z)D_A^2(z)} P_m(k = \ell/D_A, z), \quad (1)$$

where i and j label the redshift bins of the source galaxies. We take $N_{\text{TOM}} = 5$ and evenly space bins in redshift from a minimum redshift of $z = 0$ to a maximum redshift of $z = 3$. Increasing the number of bins beyond $N_{\text{TOM}} = 5$ adds only negligibly to the constraining power of lensing data, in accord with an analogous statement for dark energy constraints [39].

In Eq. (1), $H(z)$ is the Hubble expansion rate, $D_A(z)$ is the comoving angular diameter distance, and $P_m(k, z)$ is the matter power spectrum at wavenumber k and redshift z. In the following section, we describe our use of the publicly-available CMBFAST code to calculate $P_m(k)$ from cosmological perturbation evolution. In this case it will be more natural to work in the synchronous gauge, and transforming between different gauge systems can be accomplished straightforwardly by following, for example, the methods described in Ref. [40].

The W_i are the lensing weight functions for source galaxies in redshift bin i. In practice, the galaxies will be binned by photometric redshift, so that the bins will have non-trivial overlap in true redshift (see Refs. [39, 41] for detailed discussions). Defining the true redshift distribution of source galaxies in the ith photometric redshift bin as dn_i/dz, the weights are

$$W_i(z) = \frac{3}{2}\Omega_M H_0^2 (1+z) D_A(z) \int dz' \frac{D_A(z, z')}{D_A(z')} \frac{dn_i}{dz'} \quad (2)$$

where $D_A(z, z')$ is the angular diameter distance between redshift z and z' and H_0 is the present Hubble rate.

We model the uncertainty induced by utilizing photometric galaxy redshifts with the probability function of assigning an individual source galaxy photometric redshift z_p given a true redshift z, $P(z_p|z)$. The true redshift distribution of sources in the ith photometric redshift bin is

$$\frac{dn_i(z)}{dz} = \int_{z_{p,i}^{(low)}}^{z_{p,i}^{(high)}} dz_p \frac{dn(z)}{dz} P(z_p|z) \quad (3)$$

Here we take the true redshift distribution to be

$$\frac{dn(z)}{dz} = \bar{n} \frac{4z^2}{\sqrt{2\pi z_0^3}} \exp[-(z/z_0)^2] \quad (4)$$

with $z_0 \simeq 0.92$, so that the median survey redshift to $z_{med} = 1$, and $\bar{n}$ as the total density of source galaxies per unit solid angle [42–44]. We assume that uncertain photometric redshifts can be approximated by taking

$$P(z_p|z) = \frac{1}{\sqrt{2\pi}\sigma_z} \exp\left[-\frac{(z_p - z)^2}{2\sigma_z^2}\right] \quad (5)$$

where $\sigma_z(z) = 0.05(1+z)$ [39]. Complexity in photometric redshift distributions is an issue that must be overcome to bring weak lensing constraints on cosmology to fruition (e.g., Ref. [41, 45]).

Observed convergence power spectra $\bar{P}_\kappa^{ij}(\ell)$, contain both signal and shot noise,

$$\bar{P}_\kappa^{ij}(\ell) = P_\kappa^{ij} + n_i \delta_{ij} \langle \gamma^2 \rangle \quad (6)$$

where $\langle \gamma^2 \rangle$ is the noise from intrinsic ellipticities of source galaxies, and n_i is the surface density of galaxies in the ith tomographic bin. We follow recent convention and set $\sqrt{\langle \gamma^2 \rangle} = 0.2$, subsuming additional errors on galaxy shape measurements into an effective mean number density of galaxies, $\bar{n}$. Assessments of intrinsic shape noise per galaxy may be found in, for example [27, 46, 47]. Assuming Gaussianity of the lensing field, the covariance between observables $\bar{P}_\kappa^{ij}$ and $\bar{P}_\kappa^{kl}$ is

$$C_{AB} = \bar{P}_\kappa^{ik} \bar{P}_\kappa^{jl} + \bar{P}_\kappa^{il} \bar{P}_\kappa^{jk} \quad (7)$$

where the i and j map to the observable index A, and k and l map to B such that C_{AB} is a square covariance matrix with $N_{\text{TOM}}(N_{\text{TOM}} + 1)/2$ rows and columns. We assume Gaussianity throughout this work and even in our most aggressive forecases we consider only multipoles $\ell < 3000$, at which point the Gaussian assumption and several weak lensing approximations break down [48–52].

III. DECAYING DARK MATTER MODELS

A. Evolution of the Average Properties of Unstable Dark Matter

We consider dark matter decays into another species of stable dark matter with a small mass splitting, $\text{DDM} \rightarrow \text{SDM} + \text{L}$, where L denotes a "massless" daughter particle, SDM is the stable dark matter with mass m, and DDM is the decaying dark matter with mass M. The mass loss fraction f of DDM is directly related to the kick velocity deposited to the SDM particle by $f \simeq v_k/c$ from energy-momentum conservation. The following relations are valid in the rest frame of DDM particles with the kick velocity of SDM being the velocity relative to the DDM rest frame.

For a general decay, neglecting Pauli-blocking factors and inverse decays, the rate of change in the DDM distribution function is

$$\dot{f}_{DDM}(q_{DDM}) = -\frac{aM\Gamma}{E_{DDM}} f_{DDM}(q_{DDM}), \quad (8)$$

where $\dot{f}$ denotes the partial derivative of the distribution function with respect to conformal time, $d\tau = dt/a$, Γ is the decay rate, a is the cosmological scale factor, q_{DDM} is the comoving momentum, and $E_{DDM} = \sqrt{q_{DDM}^2 + M^2 a^2}$. Specializing to two-body decays, one can show that the corresponding change to the SDM distribution function will be [20, 53]

$$\dot{f}_{SDM}(p_{SDM}) = \frac{aM^2\Gamma}{2E_{SDM}\, p_{SDM}\, p_{CM}} \int_{E_i}^{E_f} dE\, f_{DDM}(p), \quad (9)$$

where

$$E_{f,i} = \frac{1}{2} E_{SDM} m_0^2 \pm p_{SDM} p_{CM} M/m_{SDM}^2,$$

the quantity p_{CM} is the center-of-mass momentum, and $m_0^2 \equiv M^2 + m^2$.

We define the average distribution function, $f_i^0(q, \tau)$, and the perturbation to the distribution function, $\Psi_i(\vec{x}, \vec{q}, \tau)$, for each species of particle labeled by i, according to

$$f_i(\vec{x}, \vec{q}, \tau) = f_i^0(q, \tau)[1 + \Psi_i(\vec{x}, \vec{q}, \tau)] \qquad (10)$$

where i can be the DDM, SDM, or L. Since DDM particles are non-relativistic, their zero order phase-space distribution is the Maxwell-Boltzmann function. The zero order phase-space distribution function of SDM is [20, 25]

$$f_{0,SDM}(q, a) = \frac{\Gamma \Omega_M \rho_{crit}}{M q^3 H(a')} \exp(-\Gamma t_q) \, \Theta(a p_{CM} - q) \quad (11)$$

where q is the comoving momentum of the SDM particle, $a' = q/p_{CM}$, and $t_q = t(a')$. This can be derived from the fact that the decay always generates SDM particles with the same physical momentum p_{CM}. In the SDM distribution function, the spectrum of different momenta arises from decays at different times, designated by the cosmic scale factor a' so that $q = p_{CM}a'$. The Heaviside step function $\Theta(a p_{CM} - q)$ (see Eq. 11) enforces a cut-off $q_{max} = a p_{CM}$ at a given redshift a. This maximum momentum stems from the fact that the maximum momentum at a given redshift is from decay processes happening at that time, while SDM with lower momenta are from the earlier decays. To be explicit, the average comoving number density of SDM particles is the integral of f_0 over momentum space,

$$n_{SDM} = \int q^2 dq \, d\Omega \, f_{0,SDM}(q) \qquad (12)$$

$$\rightarrow dn_{SDM}(q) = 4\pi q^2 dq \, f_{0,SDM}(q) \qquad (13)$$

Thus $f_{0,SDM}$ can be written as

$$f_{0,SDM}(q) = \frac{dn_{SDM}(q)}{q^2 dq} = \frac{dn_{SDM}}{q^2 p_{CM} da'} = \frac{1}{H(a') q^3} \frac{dn_{SDM}}{dt'} \qquad (14)$$

$$\rightarrow f_{0,SDM}(q) = \frac{1}{M H(a') q^3} \frac{d(\rho_{DDM} a'^3)}{dt'} \qquad (15)$$

This then implies Eq. (11) after enforcing the maximum momentum at $q_{max} = a p_{CM}$.

The evolution equations for the mean energy densities in the two dark matter components are given by the integrals of Eq. 8 and Eq. 9 using the unperturbed distribution function. They read

$$\dot{\rho}_{DDM} + 3\frac{\dot{a}}{a}\rho_{DDM} = -a\Gamma\rho_{DDM} \qquad (16)$$

and

$$\dot{\rho}_{SDM} + 3\frac{\dot{a}}{a}(\rho_{SDM} + P_{SDM}) = \Gamma \frac{a m_0^2}{2M^2}\rho_{DDM} \qquad (17)$$

respectively. Given the DDM energy density, the decay product energy density $\rho_d = \rho_{SDM} + \rho_L$ can be obtained using the first law of thermodynamics [54, 55] from

$$\frac{da^3 \rho_d}{d\tau} = -P_d \frac{da^3}{d\tau} - \frac{d(a^3 \rho_{DDM})}{d\tau}. \qquad (18)$$

This implies that the energy density evolution of the massless daughter particle L is

$$\dot{\rho}_L + 3\frac{\dot{a}}{a}(\rho_L + P_L) = \dot{\rho}_L + 4\frac{\dot{a}}{a}\rho_L = \Gamma \frac{a(M^2 - m^2)}{2M^2}\rho_{DDM} \qquad (19)$$

B. Perturbations

To compute the contemporary lensing power spectra, it is necessary to compute the perturbations to the dark matter distributions and the metric. Our treatment of perturbations follows the conventions established in Ma and Bertschinger [56]. We will present our results in the synchronous gauge, because this choice lends itself to numerical evaluation. In the synchronous gauge, the Fourier transform of the Boltzmann equation can be written

$$\frac{\partial \Psi}{\partial \tau} + i\frac{q}{E}(\vec{k}\cdot\hat{n})\Psi + \frac{d\ln f_0}{d\ln q}\left[\dot{\eta} - \frac{\dot{h} + 6\dot{\eta}}{2}(\hat{k}\cdot\hat{n})^2\right] = \frac{1}{f_0}\left(\frac{\partial f}{\partial \tau}\right)_C \qquad (20)$$

The DDM perturbation equations are the same as the well-known equations describing CDM (see Ref. [56]), so we will not describe them any further. The term on the right-hand side of Eq. (20) is the so-called *collisional term* representing the change in the distribution functions due to interactions (decays in our case). In the absence of non-gravitational interactions, $(\partial f/\partial \tau)_C = 0$. For the decay products, the collision terms are

$$\left(\frac{\partial f_{SDM}}{\partial \tau}\right)_C = \frac{a m_0^2 \Gamma}{2ME} f_{0,DDM}(1 + \Psi_{DDM}) \qquad (21)$$

and

$$\left(\frac{\partial f_L}{\partial \tau}\right)_C = \frac{a(M^2 - m^2)\Gamma}{2ME} f_{0,DDM}(1 + \Psi_{DDM}). \qquad (22)$$

The factors $m_0^2/(2M^2)$ and $(M^2 - m^2)/(2M^2)$ that appear in the SDM and L collision terms can be easily understood. Consider a two-body decay in the rest frame of the DDM particle, $A \rightarrow B + C$, with corresponding masses m_A, m_B, and m_C. The energies of B and C in the rest frame of A are $E_B = (m_A^2 + m_B^2 - m_C^2)/(2m_A)$ and $E_C = (m_A^2 + m_C^2 - m_B^2)/(2m_A)$. So these factors represent the ratios of energy that have been deposited into different daughter particle species.

The perturbations for the massless relativistic daughter particles may be treated in a manner analogous to that of massless neutrinos, save for the peculiar distribution function of the L. We integrate out the momentum

dependence in the distribution function by defining (in Fourier space)

$$F_L(\vec{k}, \hat{n}, \tau) = \frac{\int q^2 dq \, q f_L^0(q, \tau) \, \Psi_L(\vec{k}, q, \hat{n}, \tau)}{\int q^2 dq \, q f_L^0(q, \tau)} \qquad (23)$$

An expansion of F_L in a series of Legendre polynomials $P_l(\hat{k} \cdot \hat{n})$ has the form

$$F_L(\vec{k}, \hat{n}, \tau) = \Sigma_{l=0}^{\infty} (-i)^l (2l+1) F_{L,l}(\vec{k}, \tau) \, P_l(\hat{k} \cdot \hat{n}). \quad (24)$$

The standard synchronous gauge perturbations in density, velocity, and anisotropic stress are

$$\delta_{\mathrm{L}} = F_{L,0}, \qquad (25)$$

$$\theta_{\mathrm{L}} = \frac{3}{4} k \, F_{L,1}, \qquad (26)$$

and

$$\sigma_{\mathrm{L}} = \frac{1}{2} F_{L,2} \qquad (27)$$

respectively. Evaluating the Boltzmann equation for our Legendre polynomial expansion in Eq. (24) yields the evolution of the multipole coefficients in the conventional notation,

$$\dot{\delta}_{\mathrm{L}} = -\frac{2}{3}(\dot{h} + 2\theta_{\mathrm{L}}) + a\Gamma \frac{E_2}{M} \frac{\rho_{\mathrm{DDM}}}{\rho_{\mathrm{L}}}(\delta_{\mathrm{DDM}} - \delta_{\mathrm{L}}), \quad (28)$$

$$\dot{\theta}_{\mathrm{L}} = k^2(\frac{\delta_{\mathrm{L}}}{4} - \sigma_{\mathrm{L}}) - a\Gamma \frac{E_2}{M} \frac{\rho_{\mathrm{DDM}}}{\rho_{\mathrm{L}}}\theta_{\mathrm{L}}, \qquad (29)$$

$$\dot{\sigma}_{\mathrm{L}} = \frac{2}{15}(2\theta_{\mathrm{L}} + \dot{h} + 6\dot{\eta} - \frac{9}{4}kF_{\mathrm{L},3}) - a\Gamma \frac{E_2}{M} \frac{\rho_{\mathrm{DDM}}}{\rho_{\mathrm{L}}}\sigma_{\mathrm{L}}, \quad (30)$$

and

$$\dot{F}_{\mathrm{L},l} = \frac{k}{2l+1}[lF_{\mathrm{L},l-1} - (l+1)F_{\mathrm{L},l+1}] - a\Gamma \frac{E_2}{M} \frac{\rho_{\mathrm{DDM}}}{\rho_{\mathrm{L}}}F_{\mathrm{L},l}, \ l \geq 3. \quad (31)$$

Here we have defined $E_1 = (M^2 + m^2)/(2M) = m_0^2/(2M)$ and $E_2 = (M^2 - m^2)/(2M)$.

The SDM must be treated differently to account for their finite mass and non-trivial velocity kicks. We expand the perturbation to the distribution function, Ψ, in a Legendre series

$$\Psi(\vec{k}, \hat{n}, q, \tau) = \sum_{l=0}^{\infty} (-\imath)^l (2l+1) \Psi_l(\vec{k}, q, \tau) P_l(\hat{k} \cdot \hat{n}). \quad (32)$$

We have dropped the "SDM" subscript on Ψ for brevity as there should be no cause for confusion in this context. Evaluating the Boltzmann evolution equation on this expansion, we obtain for the different multipoles

$$\frac{\partial \Psi_0}{\partial \tau} = -\frac{qk}{E}\Psi_1 + \frac{1}{6}\dot{h}\frac{d\ln f_{SDM,0}}{d\ln q} + a\Gamma \frac{E_1}{E} \frac{f_{DDM,0}}{f_{SDM,0}}\Psi_{DDM,0}$$
$$- a\Gamma \frac{E_1}{E} \frac{f_{DDM,0}}{f_{SDM,0}}\Psi_0, \quad (33)$$

$$\frac{\partial \Psi_1}{\partial \tau} = \frac{qk}{3E}(\Psi_0 - 2\Psi_2) - a\Gamma \frac{E_1}{M} \frac{f_{DDM,0}}{f_{SDM,0}}\Psi_1, \qquad (34)$$

$$\frac{\partial \Psi_2}{\partial \tau} = \frac{qk}{5E}(2\Psi_1 - 3\Psi_3) - (\frac{1}{15}\dot{h} + \frac{2}{5}\dot{\eta})\frac{df_{SDM,0}}{dlnq}$$
$$- a\Gamma \frac{E_1}{E} \frac{f_{DDM,0}}{f_{SDM,0}}\Psi_2, \quad (35)$$

and

$$\frac{\partial \Psi_l}{\partial \tau} = \frac{qk}{(2l+1)E}(l\Psi_{l-1} - (l+1)\Psi_{(l+1)}) - a\Gamma \frac{E_1}{M} \frac{f_{DDM,0}}{f_{SDM,0}}\Psi_l. \quad (36)$$

for $l \geq 3$.

If we restrict attention only to cases in which the mass difference between the DDM and SDM particles is small, $f = 1 - m/M \ll 1$, the SDM particle will receive an extremely non-relativistic kick velocity $v_k \simeq fc$. As we should expect, SDM behaves similarly to CDM, aside from the fact that it is endowed with a non-negligible distribution of momentum due to the DDM decays. In this limit, the SDM perturbations evolve as for a standard non-relativistic dark matter species,

$$\dot{\delta}_{SDM} = -\theta_{SDM} - \frac{1}{2}\dot{h} + a\Gamma \frac{E_1}{M} \frac{\rho_{DDM}}{\rho_{SDM}}(\delta_{DDM} - \delta_{SDM}) \quad (37)$$

and

$$\dot{\theta}_{SDM} = -\frac{\dot{a}}{a}\theta_{SDM} + \frac{\delta P_{SDM}}{\delta \rho_{SDM}}k^2\delta_{SDM} - a\Gamma \frac{E_1}{M} \frac{\rho_{DDM}}{\rho_{SDM}}\theta_{SDM}, \quad (38)$$

where

$$c_s^2 = \frac{\delta P_{SDM}}{\delta \rho_{SDM}} = \frac{\frac{4\pi}{3}a^{-4}\int q^2 dq \frac{q^2}{E} f_0(q)\Psi_0}{4\pi a^{-4}\int q^2 dq E f_0(q)\Psi_0} \quad (39)$$

The higher multipole terms become negligible in the non-relativistic as they are proportional to powers of the ratio of the kinetic energy to the total energy, q/ϵ.

Though we solve the complete equations for the evolution of the SDM perturbations, the non-relativistic kick velocity approximation is valid in most of our calculations. The most interesting constraints from future surveys are relevant for models with $v_k \lesssim 10^{-3}c$ and relativistic kicks have already been ruled out for a wide range of lifetimes [22, 57].

Perturbation growth is suppressed on scales smaller than the *free-streaming* scale. The free-streaming scale is, in turn, determined by an integral of the sound speed c_s. We defer a detailed discussion of the free-streaming scale in our decaying dark matter models and its imprint on the matter and lensing power spectra to § VI.

IV. NONLINEAR CORRECTIONS TO STRUCTURE GROWTH

Our most robust constraints stem from perturbations on linear scales. However, it is interesting to estimate

the level of constraints that may be achieved by exploiting mildly nonlinear scales as is common practice in the established framework for exploring dark energy with lensing and galaxy clustering statistics [36]. Including mildly nonlinear scales improves constraints because it increases the signal-to-noise of lensing measurements and because it includes information regarding the effects of DDM on the abundance and internal structures of cluster-sized dark matter halos. We explore constraints including mildly nonlinear scales as a means of estimating the level of constraints that may be achievable after an exhaustive numerical simulation program, similar to what is being performed for dark energy [58].

We implement the nonlinear corrections to the matter and lensing power spectra using the halo model [59]. The halo model is known to exhibit mild systematic offsets compared to numerical simulations and the nonlinear correction of Ref. [60]. However, we use the halo model because it provides a convenient framework for estimating the alterations to nonlinear structure induced by DDM before performing an exhaustive numerical investigation. We combine the standard aspects of the halo model with an analytical model proposed by Sánchez-Salcedo [18] for the alterations to dark matter halo structure due to the kick velocities generated in the decay process.

For relevant lifetimes ($\Gamma^{-1} \gtrsim H_0^{-1}$), dark matter halos begin with the same density profiles as in the standard CDM model. Their density distributions can be well described by Navarro et al. [61] (NFW) profiles. As the DDM decays, the kinetic energy of dark matter particles will change because SDM particles receive a small kick velocity from their parent particles. Assuming that we only consider decay processes with $f \ll 1$, the mass of the parent and daughter particles will be nearly identical. As discussed in Sánchez-Salcedo [18], *on average* the net effect of decays is to impart an amount of energy $\Delta E \approx m v_k^2 / 2$ on the dark matter, independent of the initial velocity. The changes in average kinetic energy will result in changes in particle orbits, causing an expansion of dark matter halos and a shallowing of dark matter profiles.

To demonstrate the effect of density profile modification, we adopt a two-step calculation. Assume that DDM particles in halos follow circular orbits prior to any significant DDM decays. The particles orbit in the gravitational potential of the NFW halo, which can be approximately described by a power law $v_c(r) = v_0(r/r_0)^{1/2\beta}$ over any sufficiently small range of r. In a given time interval, a small fraction of DDM particles decay and their daughter SDM particles gain a small amount of energy $\Delta E \approx m v_k^2 / 2$. In general, the daughter particles will move from circular orbits to elongated orbits, characterized by the new energy relative to the halo potential and an apocentric radius r. Orbits in the NFW potential are not closed, rendering it a numerical problem to compute the time-averaged value of the radial coordinate of the daughter particle. To obtain a simplistic estimate of the new radii the particles move to, we assume that the new
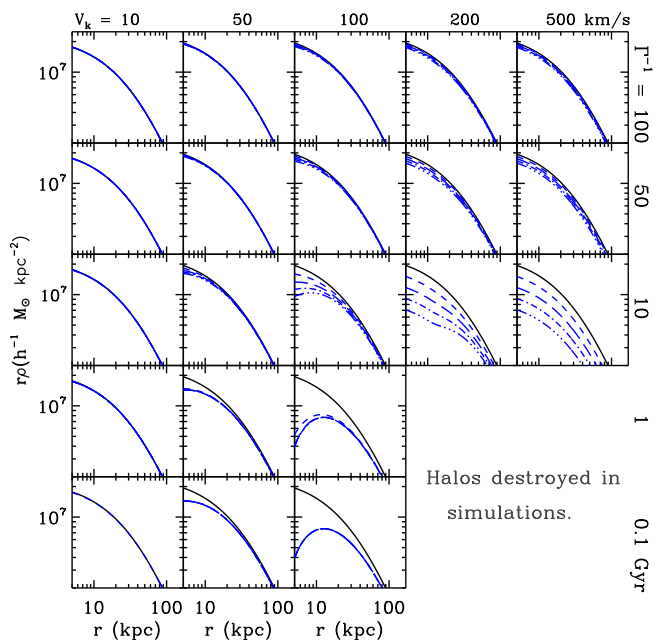

FIG. 1: Dark matter density profiles times radius, $r\,\rho(r)$, as a function of radius and time. The dark matter halo mass is $M_{\rm h} = 10^{12}\,{\rm M}_\odot$. In the absence of dark matter decays, the halo concentration is $c = 5$. The halo has a virial speed $v_{vir} \equiv \sqrt{GM_{\rm h}/R_{vir}} \approx 130$ km/s. Different panels are for different choices of kick velocity and lifetime as labeled along the top and right axes respectively. In each panel the solid lines show the initial NFW profile. The short-dashed line, long-dashed line, dash-dotted line, and dash-double-doted line represent density profiles after 2.5, 5, 7.5, and 10 Gyr. This figure is designed to be directly comparable to the simulation results displayed in Fig. 1 of Ref. [15].

average position of the daughter is similar to the radius of a circular orbit at the new value of the orbital energy. This is *conservative* in the present context, because circular orbits in equilibrium are *least* susceptible to such expansion [18]. In this assumption, the radial position of the daughter particles, r', will be

$$r' = \left(r^{1/\beta} + \frac{1}{2\beta + 1} \left(\frac{v_k(R)}{v_0} \right)^2 r_0^{1/\beta} \right)^{\beta}. \qquad (40)$$

The model we have described is not self-consistent, so it is important to validate the basic predictions of the model against more complete calculations. To check the validity of this model, we compare our analytical calculation results with the N-body simulation results from [15]. In Figure 1, we plot density profiles for a dark matter halo with mass $M_{\rm h} = 10^{12}\,{\rm M}_\odot$ and an initial NFW concentration parameter $c = 5$ for several different lifetimes and kick velocities. Peter et al. [15] computed the profiles of dark matter halos in the same model using N-body simulations that accounted for the dark matter decays. Fig. 1 above is the same as Figure 1 in Peter
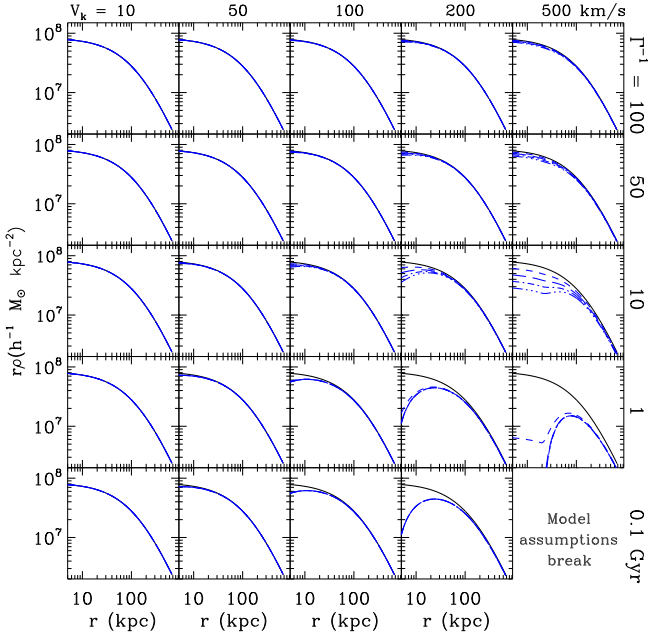
FIG. 2: Similar to Figure 1 but for halos with $M_h = 5 \times 10^{13}\,M_\odot$ and NFW concentration c=5. The halo virial speed is $v_{vir} \approx 477$ km/s.

et al. [15] save for the fact that we have computed modified halo profiles according to the analytic model described in this section. A comparison of the two figures reveals that the analytic model and the numerical simulations are in remarkable agreement for all models with $v_k \lesssim 200$ km/s and $\Gamma^{-1} \gtrsim 10$ Gyr. There are several possible explanations for the inconsistencies that arise when $v_k > 200$ km/s and $\Gamma^{-1} < 10$ Gyr. One is that when changes to the gravitational potential are not small, the final gravitational potential is sufficiently different from the initial gravitational potential that the initial potential cannot be used to approximate the new positions of the SDM particles. Another possibility is that typical circular orbits no longer provide useful approximations for the degree of halo expansion. As discussed in [15], where they look at velocity anisotropy of their simulated halos, they found that the orbits become radially biased at the halo outskirts. Moreover, $v_k = 200$ km/s is considerable compared to the virial velocity of a $M_h = 10^{12}\,M_\odot$ halo, so it is not surprising that those halos are not in dynamical equilibrium for large v_k and small lifetime. These simulation results show that the assumptions of our simple model are violated in the regime of high kick velocity and low lifetime. As we show in § VI, our primary results in which the nonlinear model is used correspond to $v_k < 200$ km/s and lifetimes $\Gamma^{-1} > 100$ Gyr, so our use of this model for a first foray into this regime is justified.

Unlike Peter et al. [15], we are interested in cosmological weak lensing as our observable. The halo mass most relevant to weak lensing lie in the range

$M_h \approx 10^{13} - 10^{14} M_\odot$ [38]. Such halos have significantly larger virial velocities than the $10^{12}\,M_\odot$ halos considered above. Typical virial velocities of these larger halos lie in the range $v_{vir} \approx 280 - 600$ km/s. This suggests that our model can be used at larger v_k than the value $v_k \approx 200$ km/s that we arrived at by comparing to simulations of a $10^{12}\,M_\odot$ halo above, because these kicks represent a smaller fraction of the potential well depth. For instance, Peter et al. [15] pointed out that the cluster mass function is insensitive to $v_k \lesssim 500$ km/s, because the typical virial speeds clusters are $v_k \gtrsim 600$ km/s. For completeness, we show the corresponding density profile modifications for these group- and cluster-sized halos in Figure 2. We will show in § VI that our calculations are only sensitive to DDM parameters that result in density profiles with mild changes.

We include this effect in our nonlinear halo model calculation by giving all recomputing halo profiles as described above prior to computing lensing correlations. We modified halo profiles by assuming initial halos with the same profiles, including concentrations, as their concordance ΛCDM counterparts and implementing the above model on these halos. The remainder of our halo model implementation follows the approach we used in Ref. [26], so we do not repeat it. Ideally, one would treat nonlinear corrections to structure growth using program of cosmological numerical simulations. However, we place such a study outside the scope of the present work as our initial aim is to estimate the constraining power of forthcoming surveys. In this manner, we estimate the fruit that a computationally-intensive numerical simulation program may bear on the problem of unstable dark matter.

V. FORECASTING METHODS

The Fisher Information Matrix provides a simple estimate of the parameter covariance given data of specified quality. The Fisher matrix has been utilized in numerous, similar contexts in the cosmology literature [26, 38, 45, 62–69], so we give only a brief review of important results and the caveats in our particular application. We have confirmed the validity of the Fisher matrix approximation in models of unstable dark matter using Monte Carlo methods as described in Ref. [26].

The Fisher matrix of observables in Eq. (1), subject to covariance as in Eq. (7), can be written as

$$F_{ij} = \sum_{\ell=\ell_{min}}^{\ell_{max}} (2\ell+1) f_{sky} \sum_{A,B} \frac{\partial P_{\kappa,A}}{\partial p_i} [C^{-1}]_{AB} \frac{\partial P_{\kappa,B}}{\partial p_j} + F_{ij}^P$$

(41)

where the indices A and B run over all $N_{\text{TOM}}(N_{\text{TOM}} + 1)/2$ spectra and cross spectra, the p_i are the parameters of the model, f_{sky} is the fraction of the sky imaged by the experiment, and $\ell_{min} = 2 f_{sky}^{-1/2}$ is the smallest multipole constrained by the experiment. F_{ij}^P is a prior

Fisher matrix incorporating previous knowledge of viable regions of parameter space. We set $\ell_{max} = 300$ for linear forecasts and $\ell_{max} = 3000$ in our most ambitious nonlinear forecasts. On smaller scales (higher ℓ), various assumptions, such as the Gaussianity of the lensing field, break down [38, 48–52, 70]. To be conservative, we explore modest priors on each parameter independently, so that $F_{ij}^P = \delta_{ij}/(\sigma_i^P)^2$, where σ_i^P is the 1σ prior on parameter p_i. The forecast, 1σ, marginalized constraint on parameter p_i is $\sigma(p_i) = \sqrt{[F^{-1}]_{ii}}$.

Our DDM model has two independent parameters, namely decay rate Γ (or lifetime, Γ^{-1}) and mass loss fraction f (which is related to v_k via $v_k = fc$). Either one of these parameters can independently be tuned to render the effects of DDM negligible, so it is not useful to marginalize over one parameter to derive constraints on the other. In what follows, we choose to illustrate the effectiveness of lensing to constrain DDM by fixing lifetime and quoting possible constraints on f. Other than the mass loss fraction f, we also consider six cosmological parameters that we expect to modify weak lensing power spectra at significant levels and to exhibit partial degeneracy with our model parameters. We construct our forecasts for DDM lifetime bounds after marginalizing over the remaining parameters. Our six additional parameters and their fiducial values (in parentheses) are the dark energy density Ω_Λ (0.74), the present-day dark matter density, $\omega_{DM} = \Omega_{DM}h^2$ (0.11), the baryon density $\omega_b = \Omega_b h^2$ (0.023), tilt parameter n_s(0.963), the natural logarithm of the primordial curvature perturbation normalization $\ln(\Delta_R^2)$ (−19.94), and the sum of the neutrino masses $\sum_i m_{\nu_i}$ (0.05 eV). This choice of fiducial model implies a small-scale, low-redshift power spectrum normalization of $\sigma_8 \simeq 0.82$. The optical depth to reionization has a negligible effect on the lensing spectra on scales of interest, so we do not vary it in our analysis.

We take priors on our cosmological parameters of $\sigma(\omega_m) = 0.007$, $\sigma(\omega_b) = 1.2 \times 10^{-3}$, $\sigma(\ln \Delta_R^2) = 0.1$, $\sigma(n_s) = 0.015$, and $\sigma(\Omega_\Lambda) = 0.03$. We assume no priors on DDM model parameters or neutrino mass. Our fiducial model is motivated by the WMAP seven-year result and our priors represent marginalized uncertainties on these parameters based on the WMAP seven-year data [4]. These priors are very *conservative* and allow for weaker constraints on DDM than would be expected from future data, where stronger priors may be available. To estimate the potential power of lensing constraints on DDM when stronger cosmological constraints are available, we also explore prior constraints on these parameters at the level expected from the Planck mission[6] using the entire Planck prior Fisher matrix of Ref. [71]. Of course, using published priors from other analyses is not self-consistent because these priors were derived in analyses that assume stable dark matter, but for rele-

vant lifetimes the dark matter decays should cause only subtle alterations to the cosmic microwave background anisotropy spectrum so this analysis should approximate a self-consistent simultaneous analysis of all data.

In some cases, we will estimate *nonlinear* power spectra in models with significant neutrino masses. In such cases, we follow the empirical prescription established in previous studies (e.g., Refs. [33, 34, 68]) and take

$$P_m(k) = \left[f_\nu \sqrt{P_\nu^{\text{lin}}(k)} + f_{b+DM} \sqrt{P_{b+DM}^{NL}(k)} \right]^2 \quad (42)$$

where

$$f_\nu = \frac{\Omega_\nu}{\Omega_m}, \quad (43a)$$

$$f_{\text{b+DM}} = \frac{\Omega_{DM} + \Omega_b}{\Omega_m}, \quad (43b)$$

$P_\nu^{\text{lin}}(k)$ is the linear power spectrum of neutrinos, and $P_{\text{b+DM}}^{\text{NL}}(k)$ is the nonlinear power spectrum evaluated for baryons and dark matter only. However, we note that recent work has questioned the robustness of this treatment of neutrino mass using direct numerical simulations [72] and perturbation theory [73], so it may become necessary to revisit this aspect of the modeling of power spectra prior to the availability of observational data.

We explore possible constraints from a variety of forthcoming data sets. We consider the Dark Energy Survey (DES) as a near-term imaging survey that could provide requisite data for this test. We model DES by taking a fractional sky coverage of $f_{sky} = 0.12$ and with $\bar{n} = 15/\text{arcmin}^2$. Second, we consider a class of future "Wide" surveys as may be carried out by the Large Synoptic Survey Telescope (LSST)[27] or Euclid [28]. We model these Wide surveys with $f_{sky} = 0.5$ and $\bar{n} = 50/\text{arcmin}^2$. Lastly, we consider a comparably narrow, deep imaging survey. We refer to such a survey as a "Deep" survey and model it with $f_{sky} = 0.05$ and $\bar{n} = 100/\text{arcmin}^2$. Such a survey may be more typical of a space-based mission similar to the proposed Wide-Field InfraRed Survey Telescope (WFIRST). In all cases, we take $\sqrt{\langle \gamma^2 \rangle} = 0.2$ and assume particular shape measurement errors from each experiment are encapsulated in their effective number densities, in accord with recent conventional practice in this regard. Our results are relatively insensitive to number density because shot noise does not dominate cosmic variance on the scales we consider, and our linear constraints are completely insensitive to the choice of galaxy number density over a wide range.

VI. RESULTS

There are several effects of DDM on lensing power spectra at low redshift. First, decays change the cosmological energy density. This change alters both structure
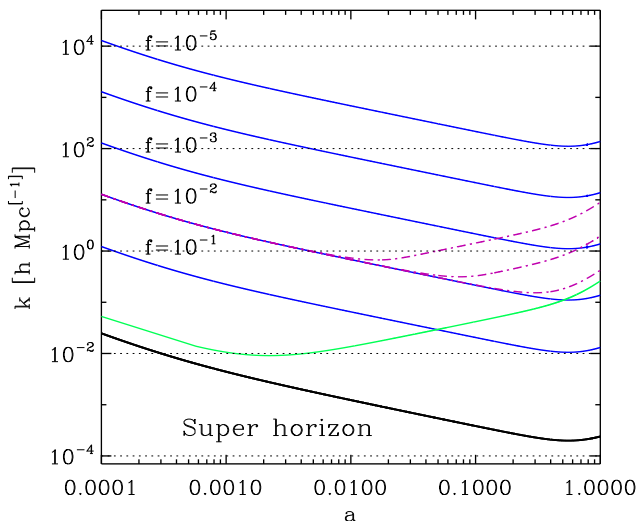
---

[6] http://www.esa.int/planck

FIG. 3: Free-streaming scale as a function of scale factor. The blue lines show free-streaming scales for lifetime much greater than the age of universe (> 100 Gyr) for several different mass loss fractions. The dash-dotted magenta lines are for $f = 10^{-2}$ and three lifetimes. From top-to-bottom at right, these are 0.01 Gyr, 0.1 Gyr, and 1 Gyr. The green line is the free-streaming scale for massive neutrino with $m_{\nu,i}$ =0.4 eV. Structure grows on scales between the free-streaming scale and horizon. On scales smaller than free-streaming scale ($k > k_{FS}$), structure growth is suppressed.

growth and distance. Further, decaying dark matter results in significant free-streaming of daughter SDM particles. While each of these effects can be important, for models near the limit of what may be constrained by lensing surveys, it is the effect of free-streaming that largely determines the lensing power spectra. In this case, the free-streaming velocity of SDM suppresses structure growth on scales smaller than free-streaming scale, an effect similar to that caused by massive neutrinos. In § VI A we show the behavior of the free-streaming scale in our model and compare it with massive neutrinos. We follow this by showing the alterations to lensing power spectra in § VI B. Our final results are the forecast constraints on DDM, which we give in § VI C.

A. Free-streaming Scale

In the standard cosmological scenario, matter density fluctuations at a particular scale grow once the scale enters the horizon ($k > H$) during the matter-dominated epoch. However, species with non-negligible primordial velocities will be able to escape the potential wells and suppress the formation of structure. The scale that corresponds to this effect is the free-streaming scale k_{FS},

which can be defined as

$$k_{FS}(a) = \sqrt{\frac{3}{2}} \frac{\mathcal{H}(a)}{c_s(a)}, \qquad (44)$$

where $\mathcal{H}(a) = a\,\mathrm{d}a/\mathrm{d}\tau$ and $\mathcal{H}^{-1}$ is the comoving horizon scale.

We show the evolution of free-streaming scale of SDM particles as a function of scale factor in Figure 3 for several mass loss fractions f and lifetimes. As discussed in [25], the behavior of the free-streaming scale of DDM can be divided into two regimes. When the decay process is still occurring, corresponding to cosmological times less than the decay lifetime, daughter particles with the same physical momentum are continuously created so that the sound speed stays approximately the same. In this case, the evolution of free-streaming scale will simply trace the evolution of horizon. If decays have ceased, which will happen when $\Gamma^{-1} < H_0^{-1}$, the sound speed will decrease as $c_s \propto a^{-1}$. The free-streaming scale shrinks as the initial velocities are red-shifted away. This effect also happens to massive neutrinos as they become non-relativistic. At early times the neutrino free-streaming scale traces the horizon so long as the neutrinos have relativistic velocities. In Figure 3 we can see that after neutrinos become non-relativistic, at $a_{nr} \simeq 1.3 \times 10^{-3}\,(0.4\,\mathrm{eV}/m_\nu)$, their free-streaming scale varies as $k_{FS} \propto a^{1/2}$ during matter domination, which is identical to free-streaming in the small lifetime limit of DDM.

B. Weak lensing Power Spectrum

As we mentioned above, DDM affects lensing power spectra in two respects. First, the power spectra for potential and density fluctuations are modified by the free streaming of the daughter SDM particles. At $k \gtrsim k_{FS}$, structure growth is suppressed. Second, the matter density is reduced as decays occur, slightly suppressing the late-time growth of structure. In the left panel in Figure 4, we show that significant decrements in power occur at roughly the same scale, $k \gtrsim 10^{-2}h\,\mathrm{Mpc}^{-1}$ for a variety of lifetimes, so long as the lifetime $\Gamma^{-1} \gg H_0^{-1}$ (the regime most relevant to our work). This suppression is due to free streaming and indeed, the scale on which the suppression occurs agrees with the estimates of the free-streaming scale shown in Fig. 3. The right panel of Fig. 4 illustrates that the scale of suppression is determined by the mass-loss fraction f, in the limit that $\Gamma^{-1} \gg H_0^{-1}$. In models with larger f, the velocities of the daughter SDM particles are higher, so at fixed lifetime, they free-stream greater distances. Both panels in Fig. 4 show a small increment in power on large scales for models with small lifetimes ($\Gamma^{-1} \lesssim 50$ Gyr) and larger mass-loss fractions ($f \gtrsim 0.1$). This delineates the parameter regime for which the overall change in the energy budget begins to have a non-negligible effect on fluctuation growth. The
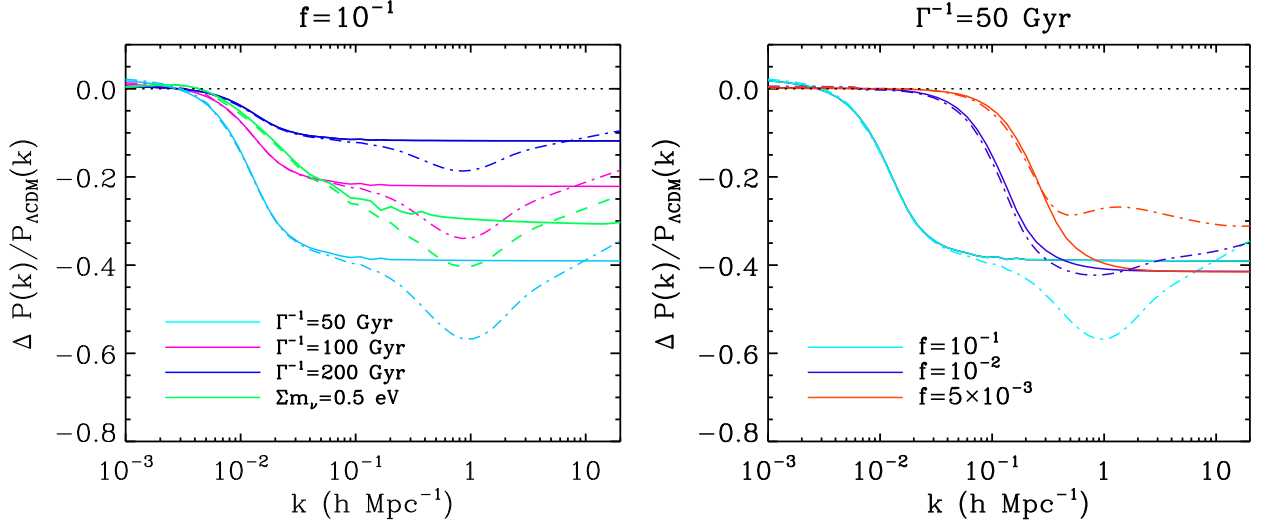
FIG. 4: Fractional difference between matter power spectrum for standard ΛCDM and a decaying dark matter model evaluated at $z = 0$. *Left*: The effect of varying the DDM lifetime at fixed mass-loss fraction, $f = 10^{-1}$. Solid curves show the linear theory predictions, and dash or dash-dot lines show predictions that include the nonlinear corrections implemented via the halo model. The green lines show the spectrum in a ΛCDM with massive neutrinos, $\Sigma m_\nu = 0.5$ eV, for comparison. *Right*: The effect of varying mass-loss fraction f, at a fixed lifetime of $\Gamma^{-1} = 50$ Gyr.

small increment on large scales in these cases enforces a fixed observed CMB normalization.

Notice in the left panel of Fig. 4 that with $f \sim 10^{-1}$, the free-streaming suppression is similar to that induced by massive neutrinos with the sum of the neutrino masses $\Sigma m_\nu \approx 0.5$ eV. This suggests that neutrinos may be degenerate with DDM, and this would be the case if it were not possible to probe a wide range of length scales and redshifts. In practice, we find that massive neutrinos are distinguishable from DDM for two reasons. First, the differences in scale dependence exhibited in Fig. 4 give a possible handle with which to separate the two. More importantly, the redshift dependence of the power spectrum differs in the two models. This is most easily seen in Fig. 3. The evolution of the free-streaming scale of massive neutrinos and the free-streaming scale of DDM differs significantly. Deep, large-scale survey data that enable probes of structure at a variety of redshifts between $0 \lesssim z \lesssim 3$, as is expected of forthcoming surveys, break the potential degeneracy between massive neutrinos and DDM.

The observed strength of gravitational lensing also has a dependence upon geometry, so differences in angular diameter distance may lead to modified lensing power spectra. Changes in relative partitioning of energy among relativistic and non-relativistic species will change the evolution of the angular diameter distance. However, we consider small mass loss fractions ($f \ll 1$) and large lifetimes ($\Gamma^{-1} \gg H_0^{-1}$), so angular diameter distances are altered only by negligible amounts and, although we account for these changes, they do not provide leverage on constraining DDM. For example, for a lifetime of $\Gamma^{-1} = 50$ Gyr and $f = 10^{-1}$, Figure 4 shows that

the changes in matter power spectrum are approximately $40 - 60\%$ for $k \gtrsim 2 \times 10^{-2}\, h\,\mathrm{Mpc}^{-1}$). The corresponding changes in angular diameter distances are less than 0.1%. The constraining power of weak lensing comes primarily from the suppression of structure growth. Incidentally, this is a promising feature because the primary information used to constrain dark energy using lensing surveys is carried by the geometric piece of the lensing signal [74, 75].

Aoyama et al. [25] have considered constraints on unstable dark matter stemming from contemporary data on the cosmological distance-redshift relations. Using constraints on the Hubble parameter, the baryon acoustic oscillation scale, and the angular positions of the cosmic microwave background anisotropy spectrum peaks, they have placed competitive constraints on such models. Aoyama et al. [25] find that $\Gamma^{-1} \gtrsim 0.1$ Gyr with $f \lesssim 3.5 \times 10^{-2}$ and that $\Gamma^{-1} \gtrsim 30$ Gyr when $f \sim 1$.

The Dash-dotted lines in Figure 5 exemplify the alterations to the small-scale lensing convergence power spectra incurred when we account for the altered halo profiles that result from dark matter decays. As f increases, kick velocities increase, and the fractional power decrement increases, as we should expect. This additional suppression is confined to relatively small scales (large multipoles, $\ell \gtrsim 300$) for most of the parameter space of interest ($v_k \lesssim 200$ km/s for $\Gamma^{-1} \lesssim 100$ Gyr).

As we pointed out in right panel in Figure 4, DDM may partially mimic massive neutrinos if redshift evolution information in not accessible. In Figure 6, we show a comparison of the redshift evolution of DDM and massive neutrino lensing power spectra in three tomographic redshift bins. Other than the difference in shapes, it is also
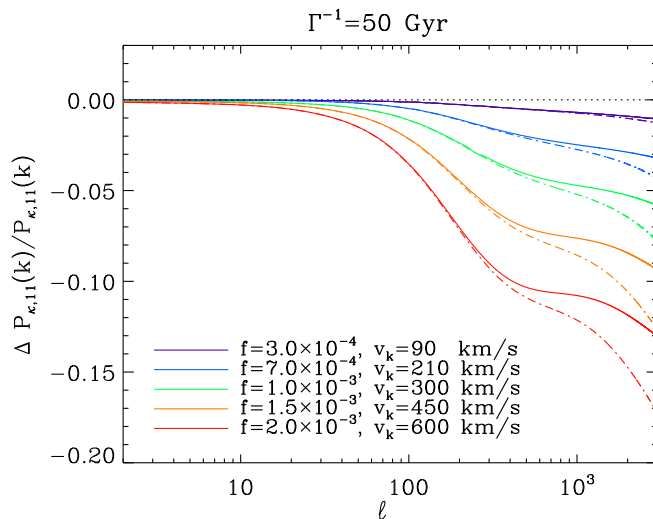
FIG. 5: Fractional difference of auto convergence lensing power spectrum between standard ΛCDM model and decaying dark matter model from first tomographic redshift bin (lensing source galaxies between $0 < z_p < 0.6$, where z_p is photometric, and not necessarily true redshift). Solid lines are calculated using halo model with NFW profiles. These lines include the alteration of the linear power spectrum on large-scales and the reduction in the abundance of dark matter halos due to free-streaming. However, halos are assumed to have the same profiles as they would in standard ΛCDM. The Dash-dotted lines include the nonlinear corrections to halo density profiles.

evident that the DDM power spectra evolve significantly more than the spectra in massive neutrino models. The reason is that the decay process continuously deposits kinetic energy into the daughter dark matter distribution, in contrast to the neutrinos which have purely redshifting kinetic energy distributions.

C. Forecast Constraints on DDM Model Parameters

To estimate of the power of weak lensing to constrain DDM, we adopt a variety of possible strategies. First, we consider constraints from data on scales where linear evolution of density fluctuations should be valid. The value of this approach is that exploiting linear scales to constrain DDM does not require a simulation program to confirm or refine nonlinear models of structure formation in these models. This can be done with contemporary theoretical knowledge of the phenomenology of these models. Moreover, relatively large-scale constraints are less observationally challenging because they exploit data on scales where cosmic variance, rather than galaxy shape measurements, are the dominant error [26]. In both cases, these constraints are conservative so we should expect that forthcoming lensing surveys designed
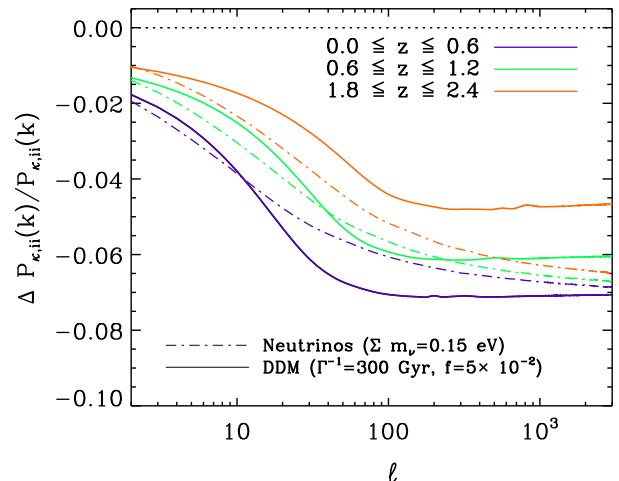
FIG. 6: Comparison of the redshift evolution of decaying dark matter and massive neutrino lensing power spectra. We plot fractional difference of auto convergence lensing power spectra between standard ΛCDM model and decaying dark matter (or massive neutrino) models in three tomographic redshift bins (labeled at the top). For simplicity, we show only the linear power spectra in this plot, though spectra computed with our nonlinear model lead to a similar conclusion.

to address dark energy should do *at least as well as our linear forecasts*. To limit ourselves to linear scales, we take data on multipoles $\ell < 300$. All of the constraints that we show in this section have been marginalized over the remaining cosmological parameters, including neutrino mass.

To show the maximum potential of lensing surveys, we consider measurements that extend into the mildly nonlinear regime, as is commonly done for dark energy forecasts. The primary value of this extension is not that particular features in the power spectra induced by DDM are added to the data set. Rather the primary improvement in constraints comes from an increase in the signal-to-noise with which the power suppression can be detected [26]. In this case, we include information on multipoles up to our quoted maximum multipole $\ell_{max} = 3000$ (see § V). Constraints on these scales will rely on reliable modeling of clustering on mildly nonlinear scales, so a comprehensive simulation program will be necessary to ensure the robustness of such constraints. A comprehensive program is computationally-intensive and beyond the scope of our present paper, as part of our goal is to emphasize that such a large-scale numerical program may be interesting and useful.

In Figure 7 we display our forecast 1σ exclusion contours alongside a variety of other contemporary constraints. The most relevant contemporary constraints come from modifications to the structures of dark matter halos with virial velocities similar to the SDM kick velocities [15] (orange region). Additional constraints may be placed on unstable dark matter by examining the proper-
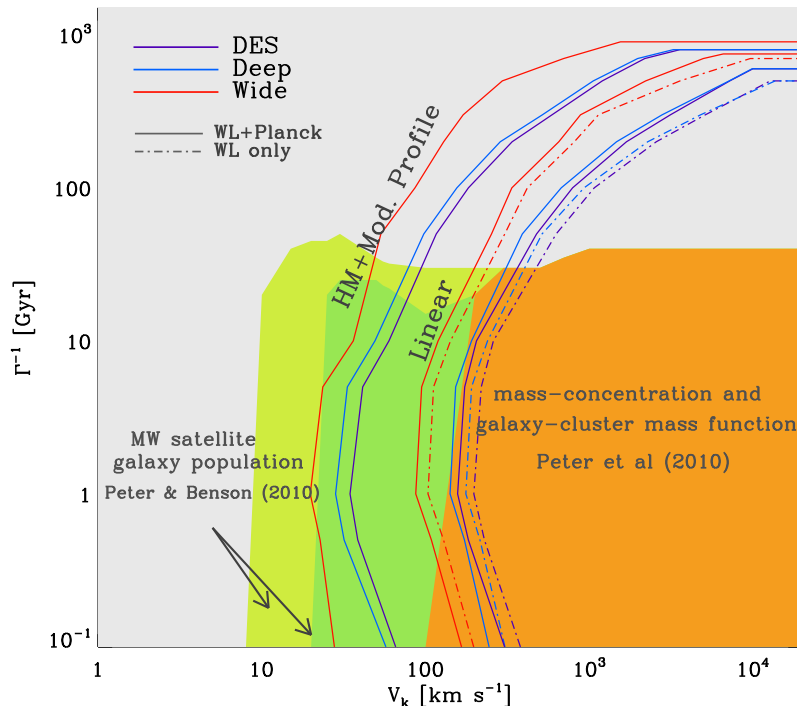
FIG. 7: Comparison of DDM parameter exclusion contours from Peter et al. [15] (orange) and Peter and Benson [22] (dark and light green) to those that may be achieved from weak gravitational lensing. The exclusions in [22] rely on a variety of assumptions regarding the merger history and formation histories of galaxies. Roughly speaking these parameter regimes also correspond to parameter values for which the interpretation of the missing satellites problem may be significantly altered by unstable dark matter (see Ref. [22] for details). The red, blue, and purple lines are the 1 σ exclusion contours from our weak lensing forecasts assuming "wide," "deep," and DES like galaxy imaging surveys respectively. The solid lines combine weak lensing with projected Planck constraints, and the dot-dash lines are from weak lensing alone. The less restrictive set of contour lines correspond to weak lensing constraints using scales on which linear theory is applicable ($\ell < 300$). The more restrictive set of contours incorporate multipoles up to $\ell_{\max} = 3000$ and the theoretical calculation includes our nonlinear corrections to halo density profiles.

ties of the satellite galaxies of the Milky Way [22] (green regions). However, these constraints rely on a variety of assumptions regarding the formation and evolution of relatively small galaxies. Moreover, these constraints delineate a range of DDM parameters for which unstable dark matter may have a significant effect on the interpretation of the missing satellites problem. As this type of DDM model has been invoked to mitigate the "missing satellite" problem, it should not be a surprise that stronger constraints also come from these types of observations. As such, it is this parameter range for which it is most interesting to develop independent constraints on unstable dark matter and that is the purpose of our weak lensing study.

As indicated in Figure 7, our most conservative, linear calculation can already give interesting constraints DDM that are competitive with contemporary bounds. The largest advantage of lensing constraints will be that it can extend constraints on DDM lifetimes significantly, as is evident in Fig. 7. These forecasts are not dependent upon modeling nonlinear structure growth, so they

constitute a robust lower limit to the constraining power of imaging surveys. Moreover, these constraints are not subject to any particular assumptions regarding the evolution and formation of galaxies, particularly the Milky Way satellite galaxies that are the subject of so much contemporary research. Comparing the linear constraints from the three types of surveys, the "Deep" survey provides slightly more restrictive constraints than DES. A "Wide" survey similar to LSST or Euclid has the potential to improve the constraints relative to DES by ∼40-60%.

The slope of the constraint contours turns over near lifetimes of a few Gyr. This turn over reflects the turn over in free streaming scale exhibited by the dash-dotted lines in Fig. 3. In models with $\Gamma^{-1} \ll H_0^{-1}$, the free-streaming scale at low redshift decreases with time. Notice that including Planck priors yields only a marginal improvement on the forecast constraints, ∼ 15−40% over the parameter ranges of interest. Our nonlinear forecasts exhibit a similar sensitivity to Planck priors, though they are not depicted in Fig. 7 in the interest of clarity.

Our more ambitious approach is to estimate constraints including data on mildly nonlinear scales. As we have already mentioned, forecast constraints in this case are less robust because they rely on data in a regime on which systematic errors and galaxy shape noise, as opposed to cosmic variance, will likely be the largest errors and because theoretical models of structure growth on these scales will need to be validated using a large suite of cosmological structure formation simulations. The most ambitious constraint forecasts in Fig. 7 result from including multipoles $\ell \leq \ell_{\max} = 3000$ along with Planck priors on the standard cosmological parameters. These forecasts indicate that weak lensing constraints on v_k that include mildly nonlinear scales may improve upon the minimal, linear constraints by nearly an order of magnitude. In this case, it is clear that weak lensing may provide an independent and competitive constraint on DDM and that lensing constraints will extend to significantly longer lifetimes than contemporary bounds.

VII. DISCUSSION AND CONCLUSION

In this paper we have explored the effect of decaying dark matter on the large-scale matter distribution and the power of future weak lensing surveys to place constraints on DDM lifetimes and mass splittings. The mass difference is parameterized by the velocity kick (v_k) that the daughter, stable dark matter particles receive upon the decay of the heavier, parent DDM. DDM leads to a suppression of matter clustering on scales below the free-streaming scale of the stable, daughter dark matter particles and this suppression can be probed with data from galaxy imaging surveys.

Our most conservative constraint forecasts result from considering lensing over large scales on which linear theory should be valid. In this case, best limits which come from a "Wide" survey, similar to Euclid or LSST. These surveys may exclude $v_k \gtrsim 90$ km/s for $\Gamma^{-1} \sim 1-5$ Gyr, a result that is competitive with contemporary constraints [15]. Lensing improves upon contemporary constraints most markedly for large decay lifetimes ($\Gamma^{-1} > H_0^{-1}$). In this regime, lensing constraints are significantly more restrictive than contemporary bounds from halo structure. In the relatively near-term, the DES will be able to place limits of $v_k \gtrsim 160$ km/s for $\Gamma^{-1} \sim 1-5$ Gyr. Achieving constraints at this level should be achievable. First, the lensing surveys we study are under development to study dark energy already. Moreover, these constraints assume that we restrict attention only to relatively large scales on which linear perturbation theory can be used to predict lensing power, so no additional theoretical effort will be necessary.

It may be possible to derive more restrictive lensing constraints on unstable dark matter by considering the mildly nonlinear scales that are commonly considered as part of the program to constrain dark energy. Including multipoles up to $ell \sim 10^3$ increases constraining power by boosting the signal-to-noise with of the weak lensing signal on scales that are sensitive to the dynamics of the dark matter. Exploiting such scales will rely on an exhaustive simulation program to understand nonlinear clustering in DDM models, similar to the simulation program that is being performed in support of dark energy probes [58], so significant additional theoretical work will be necessary. Nevertheless, the payoff may be significant. In order to estimate the ambitious constraints that may be achieved from such a data analysis, we have implemented nonlinear corrections to lensing power using the standard halo model coupled with a simple model for the modification of halo density structures due to decaying dark matter.

In our most ambitious forecasts, we find that weak lensing may constrain the mass splitting of the DDM nearly an order of magnitude more restrictively than implied by our linear scale analysis. These results suggest that weak lensing surveys will be sensitive to $v_k \sim 10$ km/s for lifetimes $\Gamma^{-1} \lesssim 10$ Gyr for all the survey types that we have considered. These constraints are interesting because they restrict parameters for which considerable effects due to DDM may be evident in the Milky Way satellite galaxy population. It may be possible to achieve similar constraints depending upon a variety of assumptions regarding the formation process of these satellite galaxies [22], but lensing provides a complementary constraint using data on distinct length scales.

We have demonstrated that measurements of the large-scale matter distribution through a weak lensing survey will be a powerful probe of decaying dark matter. This probe is valuable for several reasons. First, such surveys as PanSTARRS, LSST, DES, Euclid, and WFIRST are already being undertaken as part of the effort to constrain dark energy. The survey requirements specified by the dark energy program are the same that we assume here, so no additional observational work will be necessary. Moreover, we have shown that such measurements can provide independent, competitive constraints on models of DDM that could alter our interpretation of the small-scale problems of the standard cosmological model, particularly the missing satellites problem. In fact, we have demonstrated that lensing will probe DDM models with lifetimes that exceed contemporary bounds by an order of magnitude. Our most ambitious constraint forecasts rely upon the development of accurate and precise models of matter clustering in models of unstable dark matter. This will likely require a significant simulation effort to ensure the robustness of any constraints derived from forthcoming data. It is our hope that this proof-of-concept work will motivate more detailed numerical studies of unstable dark matter models as well as additional possible constraints from related observations.

Acknowledgments

[1] G. Jungman, M. Kamionkowski, and K. Griest, Phys. Rep. **267**, 195 (1996), arXiv:hep-ph/9506380.

[2] K. Griest and M. Kamionkowski, Phys. Rep. **333**, 167 (2000).

[3] G. Bertone, D. Hooper, and J. Silk, Phys. Rep. **405**, 279 (2005), arXiv:hep-ph/0404175.

[4] E. Komatsu, K. M. Smith, J. Dunkley, C. L. Bennett, B. Gold, G. Hinshaw, N. Jarosik, D. Larson, M. R. Nolta, L. Page, et al., Astrophys. J. Suppl. Ser. **192**, 18 (2011), arXiv:1001.4538.

[5] A. Klypin, A. V. Kravtsov, O. Valenzuela, and F. Prada, Astrophys. J. **522**, 82 (1999), astro-ph/9901240.

[6] B. Moore, S. Ghigna, F. Governato, G. Lake, T. Quinn, J. Stadel, and P. Tozzi, Astrophys. J. Lett. **524**, L19 (1999), arXiv:astro-ph/9907411.

[7] W. J. G. de Blok and A. Bosma, Astron. Astrophys. **385**, 816 (2002), arXiv:astro-ph/0201276.

[8] J. D. Simon, A. D. Bolatto, A. Leroy, L. Blitz, and E. L. Gates, Astrophys. J. **621**, 757 (2005), arXiv:astro-ph/0412035.

[9] R. Kuzio de Naray, S. S. McGaugh, and W. J. G. de Blok, Astrophys. J. **676**, 920 (2008), 0712.0860.

[10] P. Colín, V. Avila-Reese, and O. Valenzuela, Astrophys. J. **542**, 622 (2000), arXiv:astro-ph/0004115.

[11] P. Bode, J. P. Ostriker, and N. Turok, Astrophys. J. **556**, 93 (2001), arXiv:astro-ph/0010389.

[12] M. Lovell, V. Eke, C. Frenk, L. Gao, A. Jenkins, T. Theuns, J. Wang, A. Boyarsky, and O. Ruchayskiy, ArXiv e-prints (2011), arXiv:1104.2929.

[13] A. R. Zentner and J. S. Bullock, Phys. Rev. D **66**, 043003 (2002), arXiv:astro-ph/0205216.

[14] A. R. Zentner and J. S. Bullock, Astrophys. J. **598**, 49 (2003), arXiv:astro-ph/0304292.

[15] A. H. G. Peter, C. E. Moody, and M. Kamionkowski, ArXiv e-prints (2010), arXiv:1003.0419.

[16] D. N. Spergel and P. J. Steinhardt, Physical Review Letters **84**, 3760 (2000), arXiv:astro-ph/9909386.

[17] A. H. G. Peter, Phys. Rev. D **81**, 083511 (2010), arXiv:1001.3870.

[18] F. J. Sánchez-Salcedo, The Astrophysical Journal Letters **591**, L107 (2003), arXiv:astro-ph/0305496.

[19] R. Cen, Astrophys. J. Lett. **546**, L77 (2001), arXiv:astro-ph/0005206.

[20] M. Kaplinghat, Phys. Rev. D **72**, 063510 (2005), arXiv:astro-ph/0507300.

[21] M. Abdelqader and F. Melia, Mon. Not. R. Astron. Soc. **388**, 1869 (2008), 0806.0602.

[22] A. H. G. Peter and A. J. Benson, Phys. Rev. D **82**, 123521 (2010), 1009.1912.

[23] N. F. Bell, A. J. Galea, and K. Petraki, Phys. Rev. D **82**, 023514 (2010), arXiv:1004.1008.

[24] N. F. Bell, A. J. Galea, and R. R. Volkas, Phys. Rev. D **83**, 063504 (2011), arXiv:1012.0067.

[25] S. Aoyama, K. Ichiki, D. Nitta, and N. Sugiyama, ArXiv e-prints (2011), arXiv:1106.1984.

[26] M.-Y. Wang and A. R. Zentner, Phys. Rev. D **82**, 123507 (2010), 1011.2774.

[27] L. S. Collaborations, arXiv:0912.0201 (2009).

[28] A. Refregier, A. Amara, T. D. Kitching, A. Rassat, R. Scaramella, J. Weller, and f. t. Euclid Imaging Consortium, ArXiv:1001.0061 (2010).

[29] B. A. Reid, W. J. Percival, D. J. Eisenstein, L. Verde, D. N. Spergel, R. A. Skibba, N. A. Bahcall, T. Budavari, J. A. Frieman, M. Fukugita, et al., Mon. Not. R. Astron. Soc. **404**, 60 (2010), arXiv:0907.1659.

[30] U. Seljak, A. Makarov, P. McDonald, and H. Trac, Physical Review Letters **97**, 191303 (2006), arXiv:astro-ph/0602430.

[31] A. Boyarsky, J. Lesgourgues, O. Ruchayskiy, and M. Viel, Journal of Cosmology and Astro-Particle Physics **5**, 12 (2009), arXiv:0812.0010.

[32] M. Viel, M. G. Haehnelt, and V. Springel, JCAP **6**, 15 (2010), arXiv:1003.2422.

[33] S. Hannestad, H. Tu, and Y. Y. Wong, Journal of Cosmology and Astro-Particle Physics **6**, 25 (2006), arXiv:astro-ph/0603019.

[34] K. Ichiki, M. Takada, and T. Takahashi, Phys. Rev. D **79**, 023520 (2009), arXiv:0810.4921.

[35] K. Markovic, S. Bridle, A. Slosar, and J. Weller, JCAP **1**, 22 (2011), arXiv:1009.0218.

[36] A. Albrecht, G. Bernstein, R. Cahn, W. L. Freedman, J. Hewitt, W. Hu, J. Huth, M. Kamionkowski, E. W. Kolb, L. Knox, et al., ArXiv Astrophysics e-prints (2006), astro-ph/0609591.

[37] D. Huterer, arXiv:1001.1758 (2010).

[38] A. R. Zentner, D. H. Rudd, and W. Hu, Phys. Rev. D **77**, 043507 (2008), arXiv:0709.4029.

[39] Z. Ma, W. Hu, and D. Huterer, Astrophys. J. **636**, 21 (2006), astro-ph/0506614.

[40] C. Ma and E. Bertschinger, Astrophys. J. **455**, 7 (1995), arXiv:astro-ph/9506072.

[41] A. P. Hearin, A. R. Zentner, Z. Ma, and D. Huterer, Astrophys. J. **720**, 1351 (2010), arXiv:1002.3383.

[42] I. Smail, D. W. Hogg, L. Yan, and J. G. Cohen, Astrophys. J. Lett. **449**, L105+ (1995), arXiv:astro-ph/9506095.

[43] I. Smail, R. S. Ellis, M. J. Fitchett, and A. C. Edge, Mon. Not. R. Astron. Soc. **273**, 277 (1995), arXiv:astro-ph/9402049.

[44] J. A. Newman, Astrophys. J. **684**, 88 (2008), arXiv:0805.1409.

[45] G. Bernstein and D. Huterer, Mon. Not. R. Astron. Soc. **401**, 1399 (2010), arXiv:0902.2782.

[46] R. Massey, J. Rhodes, A. Refregier, J. Albert, D. Ba-

con, G. Bernstein, R. Ellis, B. Jain, T. McKay, S. Perlmutter, et al., Astron. J. **127**, 3089 (2004), arXiv:astro-ph/0304418.

[47] M. M. Kasliwal, R. Massey, R. S. Ellis, S. Miyazaki, and J. Rhodes, Astrophys. J. **684**, 34 (2008), 0710.3588.

[48] M. White and W. Hu, Astrophys. J. **537**, 1 (2000).

[49] A. Cooray and W. Hu, Astrophys. J. **554**, 56 (2001), astro-ph/0012087.

[50] C. Vale and M. White, Apj **592**, 699 (2003).

[51] S. Dodelson, C. Shapiro, and M. White, Phys. Rev. D **73**, 023009 (2006), arXiv:astro-ph/0508296.

[52] E. Semboloni, L. van Waerbeke, C. Heymans, T. Hamana, S. Colombi, M. White, and Y. Mellier, Mon. Not. R. Astron. Soc. **375**, L6 (2007), arXiv:astro-ph/0606648.

[53] G. D. Starkman, N. Kaiser, and R. A. Malaney, Astrophys. J. **434**, 12 (1994), arXiv:astro-ph/9312020.

[54] R. E. Lopez, Ph.D. thesis, THE UNIVERSITY OF CHICAGO (1999).

[55] E. Kolb and M. Turner, *The Early Univrse* (Westview Press, 1994).

[56] C. Ma and E. Bertschinger, Astrophys. J. **455**, 7 (1995), arXiv:astro-ph/9506072.

[57] A. H. G. Peter, ArXiv e-prints (2010), arXiv:1001.3870.

[58] K. Heitmann, M. White, C. Wagner, S. Habib, and D. Higdon, ArXiv:0812.1052 (2008).

[59] A. Cooray and R. Sheth, Phys. Rep. **372**, 1 (2002).

[60] R. E. Smith, J. A. Peacock, A. Jenkins, S. D. M. White, C. S. Frenk, F. R. Pearce, P. A. Thomas, G. Efstathiou, and H. M. P. Couchman, Mon. Not. R. Astron. Soc. **341**, 1311 (2003), astro-ph/0207664.

[61] J. F. Navarro, C. S. Frenk, and S. D. M. White, Astrophys. J. **490**, 493 (1997), astro-ph/9611107.

[62] G. Jungman, M. Kamionkowski, A. Kosowsky, and D. N. Spergel, Phys. Rev. D **54**, 1332 (1996), arXiv:astro-ph/9512139.

[63] M. Tegmark, A. N. Taylor, and A. F. Heavens, Astrophys. J. **480**, 22 (1997), arXiv:astro-ph/9603021.

[64] U. Seljak, Astrophys. J. **482**, 6 (1997), arXiv:astro-ph/9608131.

[65] W. Hu, Astrophys. J. Lett. **522**, L21 (1999), astro-ph/9904153.

[66] A. Kosowsky, M. Milosavljevic, and R. Jimenez, Phys. Rev. D **66**, 063007 (2002), arXiv:astro-ph/0206014.

[67] D. Huterer and M. Takada, Astroparticle Physics **23**, 369 (2005), astro-ph/0412142.

[68] T. D. Kitching, A. F. Heavens, L. Verde, P. Serra, and A. Melchiorri, Phys. Rev. D **77**, 103008 (2008), arXiv:0801.4565.

[69] A. H. G. Peter, ArXiv e-prints (2009), arXiv:0910.4765.

[70] D. H. Rudd, A. R. Zentner, and A. V. Kravtsov, Astrophys. J. **672**, 19 (2008), arXiv:astro-ph/0703741.

[71] W. Hu, D. Huterer, and K. M. Smith, Astrophys. J. Lett. **650**, L13 (2006), arXiv:astro-ph/0607316.

[72] S. Bird, M. Viel, and M. G. Haehnelt, ArXiv e-prints (2011), arXiv:1109.4416.

[73] S. Saito, M. Takada, and A. Taruya, Physical Review Letters **100**, 191301 (2008), 0801.0607.

[74] H. Zhan and L. Knox, ArXiv Astrophysics e-prints (2006), arXiv:astro-ph/0611159.

[75] A. P. Hearin and A. R. Zentner, Journal of Cosmology and Astro-Particle Physics **4**, 32 (2009), arXiv:0904.3334.